RSC Advances

PAPER

View Article Online
View Journal | View Issue

Cite this: *RSC Adv.*, 2021, **11**, 21897

Multispectral upconversion nanoparticles for near infrared encoding of wearable devices†

Gibum Lee,‡ Jonghwan Mun,‡ Hyunsik Choi, Seulgi Han and Sei Kwang Hahn *

Individual recognition technology such as iris recognition and bar coding has been extensively investigated for non-face-to-face authorization. However, there are still strong unmet needs for facile, rapid, and robust individual recognition. Here, we developed multispectral transparent films of upconversion nanoparticles (UCNPs) for near-infrared (NIR) encoding of wearable devices including contact lenses and patch devices. A multispectral UCNP film in a contact lens showed various luminescence colors of patterns under 980 nm NIR light irradiation and each color could be assigned to a specific code by RGB value analysis. The encoded film of UCNPs in the contact lens was successfully decoded by the RGB value analysis with a charge coupled digital (CCD) camera. Furthermore, the UCNP barcode film could be applied in the form of attachable barcode patches onto various substrates like porcine skin and paper currency. Taken together, we could confirm the feasibility of multispectral UCNP transparent films as a facile individual recognition platform for non-face-to-face authorization.

Received 7th May 2021
Accepted 15th June 2021

DOI: 10.1039/d1ra03572j

rsc.li/rsc-advances

Introduction

Individual recognition systems have been used for various applications including surveillance, financial transactions, access management and patient healthcare. For individual recognition, biometrics systems like iris recognition were developed for commercial non-face-to-face authorization. Due to high reliability by the distinct aspect of biometrics, these systems were used to digitally identify a person for granting access using physical or behavioral characteristics such as facial patterns, fingerprints, voice or typing cadence.[1,2] However, biometrics systems are generally cost- and time-consuming for the recognition of captured images. Moreover, the accuracy in the recognition of individual biometrics systems depends on the environment, quality, alignment, and camera performance.[3] Accordingly, a facile, fast, robust and inexpensive recognition system transparent under visible light is highly needed for various wearable device applications.

Recently, various encoding systems for individual recognition, such as graphical encoding[4,5] and spectral encoding,[6] have been investigated in order to increase coding capacities. Several particle-encoding methods were proposed for the combination of graphical and spectral encoding with dramatically expandable permutation.[7–11] For example, micro-polymeric particles were encoded by continuous flow lithography method for the detection of DNA oligomers.[12] In addition, magnetic particles were utilized for the encoding of communicating objects.[13] Especially, upconversion nanoparticles (UCNPs) are a remarkable platform as information carriers due to their unique luminescent properties such as photon upconversion with large anti-Stokes shifts, broad-spectrum, biocompatibility, ease of multifunctionality, facile size and phase tunability, and satisfactory signal output.[14–23] UCNPs have been harnessed for photomedicine,[24–27] multimodal bioimaging,[28–30] biomedical device,[31,32] molecular sensing,[33] and optical security.[34]

Here, we designed multispectral transparent films of UCNPs for simple, fast, reproducible, and highly robust near-infrared (NIR) encoding of wearable devices including contact lens and patch devices. To design the graphical/spectral hybrid encoding platform, we introduced UCNPs as a luminescent material and a contact lens and a skin patch as model wearable devices with high accessibility and wearing convenience.[35–37] The multispectral UCNPs were fabricated into transparent UCNPs barcode patterned polydimethylsiloxane (PDMS) films with a specific sequence for encoding with RGB colors. By inserting this film into the wearable contact lens, we firstly made transparent UCNPs barcode patterned contact lens (UCNPs-BCL). Upon NIR light irradiation, UCNPs-BCL can emit a specific barcode sequence of patterns which can be decoded with a charge coupled digital (CCD) camera for individual recognition (Fig. 1a). In addition, we prepared an attachable barcode patch using the transparent UCNPs barcode patterned film and applied onto various substrates like a porcine skin and a paper currency. We demonstrated the feasibility of UCNPs barcode

Department of Materials Science and Engineering, Pohang University of Science and Technology (POSTECH), 77 Cheongam-ro, Nam-gu, Pohang, Gyeongbuk 37673, Korea. E-mail: skhanb@postech.ac.kr; Fax: +82 54 279 2399; Tel: +82 54 279 2159

† Electronic supplementary information (ESI) available. See DOI: 10.1039/d1ra03572j

‡ These authors contributed equally to this work and should be considered as co-first authors.

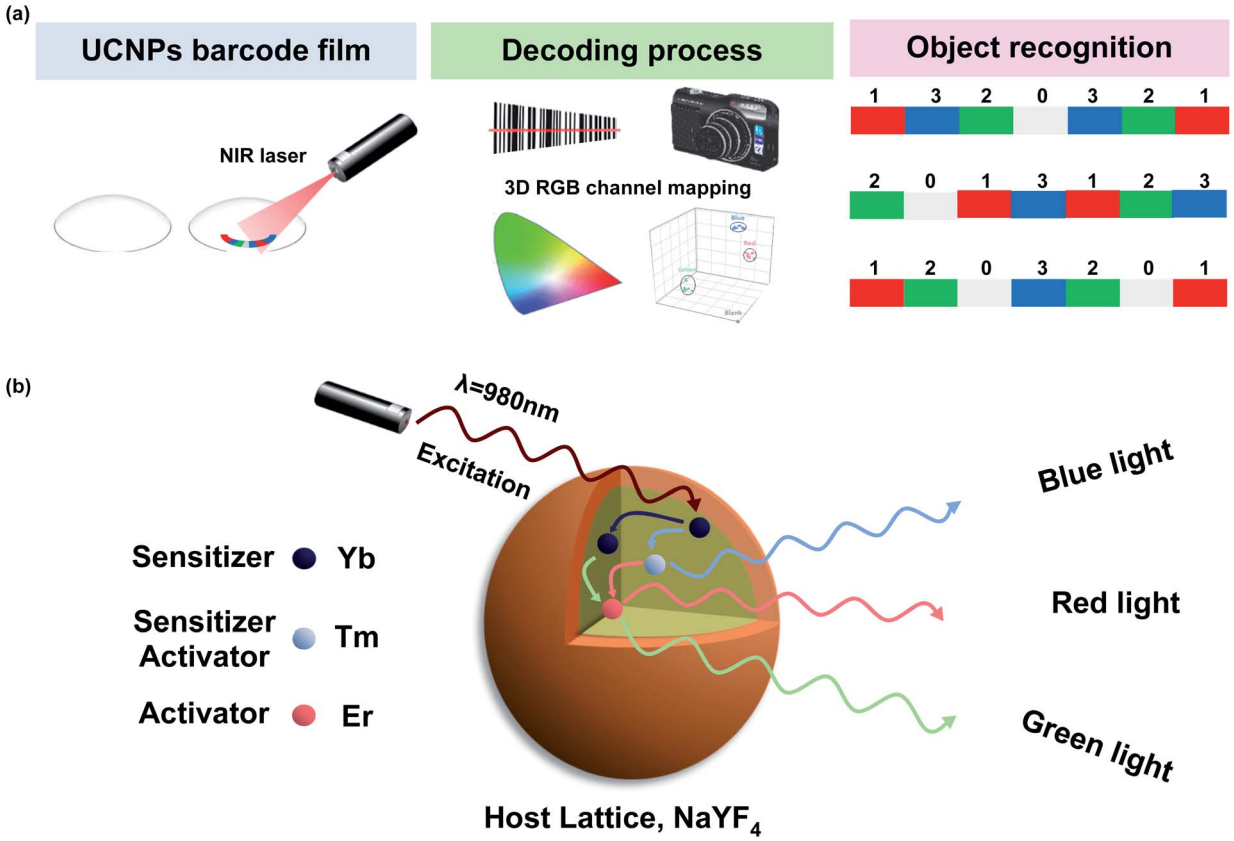

Fig. 1 (a) Schematic illustration for a NIR encoding transparent UCNPs barcode film embedded in a contact lens as a model system for wearable individual recognition, the decoding process with a CCD camera through RGB value analysis, and the relevant object recognition according to the assigned codes under 980 nm NIR light. (b) Schematic illustration for the upconversion mechanism of RGB visible light emitting UCNPs.

patterned film as a facile and robust individual recognition platform for non-face-to-face authorization.

Materials and methods

Materials

SYLGARD 184 silicone elastomer and curing agent were purchased from Dow Corning (Midland, MI) and MED-6015 silicone elastomer and curing agent were purchased from NuSil Technology (Carpinteria, CA). Lanthanide chloride hexahydrates ($YCl_3 \cdot 6H_2O$, $GdCl_3 \cdot 6H_2O$, $YbCl_3 \cdot 6H_2O$ and $TmCl_3 \cdot 6H_2O$), oleic acid (OA), octadecene-1 (ODE), ammonium fluoride (NH_4F), and cyclohexane were purchased from Sigma Aldrich (St. Louis, MO).

Methods

Synthesis of UCNPs. $NaYbF_4$:Er^{3+},Tm^{3+} (69% Yb^{3+}, 30% Er^{3+} and 1% Tm^{3+} molar ratio), $NaYF_4$:Yb^{3+},Er^{3+} (78% Y^{3+}, 20% Yb^{3+} and 2% Er^{3+} molar ratio), $NaYF_4$:Yb^{3+},Tm^{3+} (79.5% Y^{3+}, 20% Yb^{3+} and 0.5% Tm^{3+} molar ratio) core nanoparticles were synthesized as reported elsewhere.[32,40] One mmol $LnCl_3$ (Ln:Y, Yb, Tm, Er as above ratio) was dissolved in 5 mL methanol in a 250 mL three-necked flask, which was mixed with a magnetic stirrer to evaporate methanol at 70 °C. After evaporating methanol completely, 6 mL OA and 15 mL ODE were added into the flask. The mixture was heated up at 110 °C for 10 min to evaporate the remaining water under N_2 gas flow. Then, the mixture was heated up to 150 °C for 30 min to make a clear core precursor solution. After cooling down to 50 °C, 100 mg of NaOH and 160 mg of NH_4F were added, which was maintained for 30 min. The mixture was heated up again to 120 °C and maintained under N_2 gas flow for 15 min and under vacuum for 10 min to evaporate the residual water. Subsequently, the mixture was heated to 300 °C for 1 h under N_2 atmosphere and cooled down to room temperature. After centrifugation, the products were precipitated by the addition of acetone and stored in 10 mL cyclohexane for further use.

UCNPs@$NaYF_4$ core–shell nanoparticles were synthesized as reported elsewhere.[32,40] One half mmol of YCl_3 was dissolved in 5 mL methanol in a three-necked 250 mL flask, which was mixed with a magnetic stirrer to evaporate methanol at 70 °C. After evaporating methanol completely, 6 mL OA and 15 mL ODE were added into the flask. The mixture was heated up at 110 °C for 10 min to evaporate the residual water under N_2 gas flow. Then, the mixture was heated up to 150 °C for 30 min to make a clear shell precursor solution. After cooling down to 70 °C, 5 mL of core UCNPs dissolved in cyclohexane were added into the mixture, which was maintained for 10 min to evaporate cyclohexane. After cooling down to 50 °C, 100 mg NaOH and 160 mg NH_4F were added, which was maintained for 30 min.

Then, the mixture was heated again up to 120 °C and maintained under N_2 gas flow for 15 min and under vacuum for 10 min to evaporate the residual water. Subsequently, the mixture was heated to 300 °C for 1 h under N_2 atmosphere and cooled down to room temperature. After centrifugation, the products were precipitated by the addition of acetone and stored in 5 mL cyclohexane.

Characterization of UCNPs. The core and core–shell structures of UCNPs were analyzed by TEM and the composition of the UCNPs was determined by EDS (JEM-2200FS, JEOL Co., Akishima, Japan). The uniform crystal lattice of UCNPs were analyzed by XRD (8 kW D/MAX-2500V, Rigaku, Japan). The emission spectra were collected with a Fluorolog modular spectrofluorometer (FL-1039, Horiba Scientific Co.) using the excitation light source of infrared diode laser at 980 nm (SDL-980-LM-2000T, Shanghai Dream Lasers Technology Co.). UCNP emission images were taken with a Nikon D200 digital camera. The elemental mapping image of UCNPs was obtained by electron energy loss spectroscopy (EELS). The mean particle size and the shell thickness were measured by dynamic light scattering (DLS).

Preparation of UCNPs barcode film. The UCNPs solution in 0.2 mL cyclohexane was added into 1 mL silicone elastomer. Subsequently, 0.1 mL curing agent was added into the mixture, which was mixed well until generating bubbles. After the bubbles were removed in vacuum, the blended mixture was poured into a mold and aged at 80 °C for 30 min. This procedure was repeated with different emission spectral UCNPs according to the specific sequence of code and number of digits.

Encoding and decoding of UCNPs barcode film. The RGB values of UCNPs emission spectra were analyzed with a CCD camera (D7000, Nikon) and an ImageJ software. The code was assigned according to the analyzed RGB values. The images of barcode pattern with a specific sequence were taken with a CCD camera and transferred into ImageJ software to analyze RGB values in sequence. The analyzed RGB values of barcode patterns were compared with the UCNPs RGB values which previously analyzed, and the barcode pattern was decoded into the assigned code in a specific sequence under 980 nm laser (SDL-980-LM-2000T, Shanghai Dream Lasers Technology Co.).

Fabrication of contact lens with a UCNPs barcode patch. The UCNPs color lenses were fabricated by thermal polymerization of contact lens precursor solutions. The contact lens precursor solution was prepared by mixing silicone elastomer and a curing agent at a ratio of 10 : 1. The UCNPs solution in cyclohexane was added into the contact lens precursor solution at 20% (v/v). The final mixed solution (80 μL) was injected in a contact lens mold and cured at 100 °C in an oven for 30 min. In addition, the UCNPs barcode patch was fabricated and cut to fit the curvature of the contact lens for embedding at the edge of the contact lens. The precursor solution was loaded onto a contact lens shape female mold and the fabricated barcode patch of UCNPs was put at the edge of the mold. Then, the male mold was fitted to the female mold, which was cured in a 100 °C oven for 30 min. After curing, the contact lens was removed from the mold and washed with ethanol and DI water.

Results and discussion

We synthesized red (R), green (G), and blue (B) spectral emission UCNPs by modulating the doping concentrations of lanthanide rare-earth elements for the particle encoding. To enhance upconversion efficiency with surface passivation for more clear barcode patterns,[41] red (R), green (G), and blue (B) emission core–shell structured UCNPs (rUCNPs, bUCNPs, and gUCNPs) were synthesized at a high temperature of 300 °C. The emission spectra of UCNPs were well tuned by changing the doping concentration of Yb, Er and Tm. The lanthanide ion was doped through substitutional process. Y^{3+} ion in the host lattice was substituted for other Ln^{3+} ions.[38,39] UCNPs doped with a combination of sensitizer (*e.g.*, Yb^{3+}, Tm^{3+}) and activator (*e.g.*, Er^{3+}, Tm^{3+}) can be excited by 980 nm NIR light to emit upconverted light. Multiple sensitizers are excited and the energy is transferred to activators. When Yb is a sensitizer and Er or Tm is an activator, UCNPs emit green or blue light spectra, because the energy state of Er or Tm is known to produce the green or blue light, respectively. However, when coupled with both Er and Tm, Tm serves as a sensitizer with Yb, because Tm is a transient energy trapper, and an activator of Er emits red light spectra.[42]

Fig. 2 shows the characterization of UCNPs by transmission electron microscopy (TEM), electron energy loss spectroscopy (EELS), spectro-fluorometry and X-ray diffraction (XRD). TEM images show the morphology of synthesized nanoparticles of rUCNPs, gUCNPs, and bUCNPs. In addition, EELS elemental mapping images show that the particles had a core–shell structure of UCNPs with a different core element and a $NaYF_4$ inert shell (Fig. 2a–c). Dynamic light scattering (DLS) analysis showed a uniform mean core particle size of ~21 nm and a mean core–shell particle size of ~33 nm (PDI < 0.2) with a shell thickness of ~12 nm (Fig. S1†). According to the analysis by EDS, the compositions of synthesized particles were well matched with the precursor ratio (Fig. S2†). We confirmed that the synthesized UCNPs could emit sufficient RGB light upon 980 nm NIR irradiation (500 mW cm^{-2}). Fig. 2d–f show the photoimages of upconversion emission spectra of UCNPs under 980 nm NIR light (500 mW cm^{-2}). The UCNPs converted 980 nm NIR light to 350–450 nm range of blue spectra, 550 nm green spectra and 660 nm red spectra depending on the doped ratio of Er and Tm (Fig. 2g). We compared the photoluminescence (PL) intensity to confirm the upconversion luminescence enhancement by the surface passivation of $NaYF_4$ inert shell. The core–shell particles had more than 2-fold of PL intensity than core particles (Fig. S3†). According to the XRD analysis, the diffraction peaks of UCNPs (blue, green and red line) were well matched with the standard β-$NaYF_4$ diffraction peaks (black, JCPDS no. 16-0334). The XRD analysis verified the hexagonal crystal structure of rUCNPs, gUCNPs and bUCNPs. The average diameters of rUCNPs, gUCNPs and bUCNPs derived from the XRD experiments using the Scherrer's equation were about 27.6 nm, 28.3 nm and 27.9 nm, respectively.

In order to encode the unique spectroscopic characteristics of UCNPs-PDMS composites, we assessed the RGB value of each

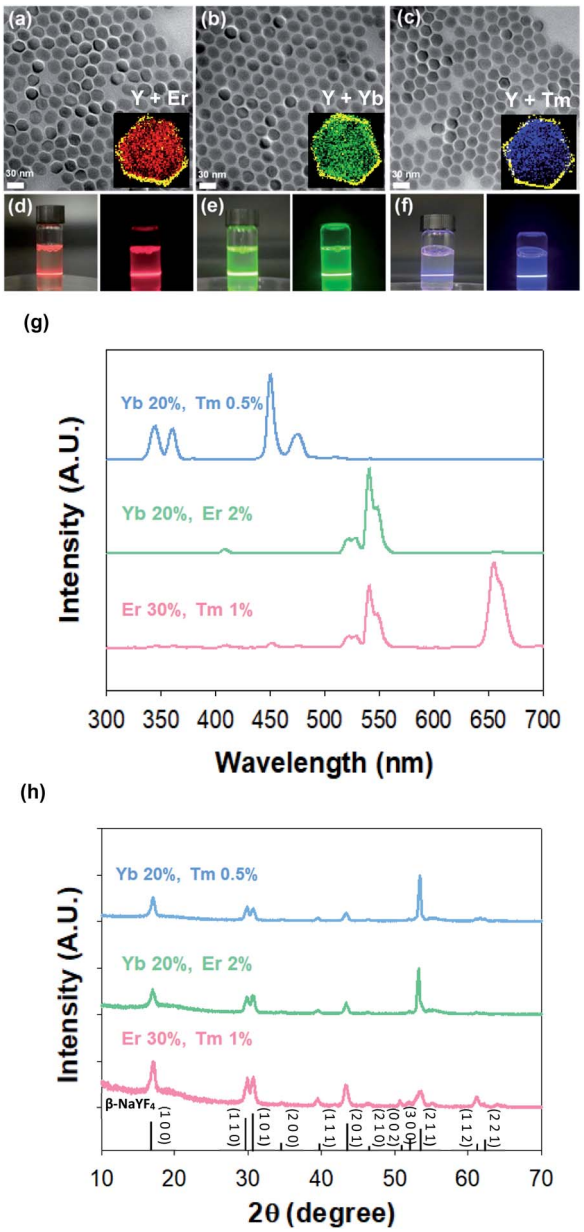

Fig. 2 Characterization of RGB emission core–shell UCNPs. TEM images of (a) $NaYbF_4$:Er,Tm@$NaYF_4$ (69% Yb, 30% Er and 1% Tm, rUCNPs), (b) $NaYF_4$:Yb,Er@$NaYF_4$ (78% Y, 20% Yb and 2% Er, gUCNPs) and (c) $NaYF_4$:Yb,Tm@$NaYF_4$ (79.5% Y, 20% Yb and 0.5% Tm, bUCNPs) (scale bar = 30 nm) with EELS image insets of Y (yellow), Yb (red), Er (green), and Tm (blue). The upconversion emission images of (d) rUCNPs, (e) gUCNPs and (f) bUCNPs under indoor-room light field and dark field. (g) Upconversion emission spectra of rUCNPs, gUCNPs and bUCNPs. (h) XRD diffraction peaks analysis of rUCNPs, gUCNPs and bUCNPs (red, green, blue) and β-$NaYF_4$, JCPDS no. 16-0334 standard diffraction peaks (black).

rUCNPs-PDMS, gUCNPs-PDMS and bUCNPs-PDMS composite. The RGB spectral emitting UCNPs-PDMS composites showed sufficient transmittance and upconversion emission patterns under 980 nm NIR as shown in Fig. 3a and b. In addition, we prepared UCNPs color lenses which could emit RGB color upon 980 nm NIR irradiation (Fig. 3c and d). These UCNPs color

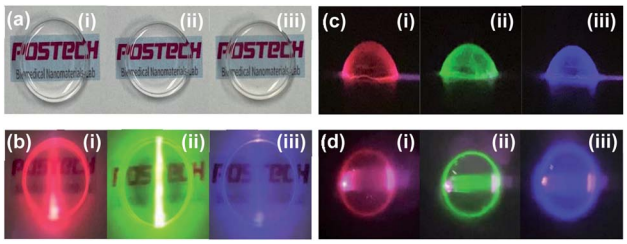

Fig. 3 (a) The photoimages and (b) the upconversion emission images under 980 nm light (500 mW cm^{-2}) of (i) rUNCPs-PDMS, (ii) gUNCPs-PDMS and (iii) bUNCPs-PDMS composites. The photoimages of UCNPs embedded color lenses: (c) side view and (d) top view under 980 nm light (500 mW cm^{-2}).

lenses would be harnessed for the beauty lens business, emitting luminescence in a dark room. Subsequently, we analyzed the optical properties by commission internationale de l'eclairage (CIE) color coordinates and the RGB value of each UCNPs-PDMS composite under 980 nm NIR light. As shown in the CIE plot, we confirmed that rUCNPs, gUCNPs and bUCNPs showed each unique spectroscopic-property (Fig. 4a). In addition, we analyzed the RGB values of UCNPs-PDMS and plotted each value in the 3D RGB channel map (Fig. 4b). We assigned unique code 1, code 2 and code 3 to rUCNPs-PDMS, gUCNPs-PDMS and bUCNPs-PDMS for each color according to the

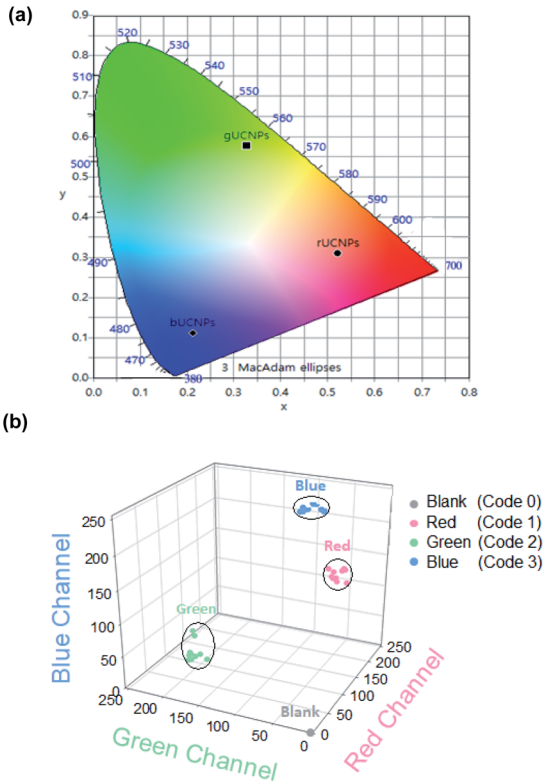

Fig. 4 (a) CIE color coordinates of rUCNP, gUCNP and bUCNP-PDMS composites. (b) The RGB values plot of red (rUNCPs-PDMS), green (gUNCPs-PDMS) and blue (bUNCPs-PDMS) in 3D RGB channel map and the assigning codes ($n = 10$).

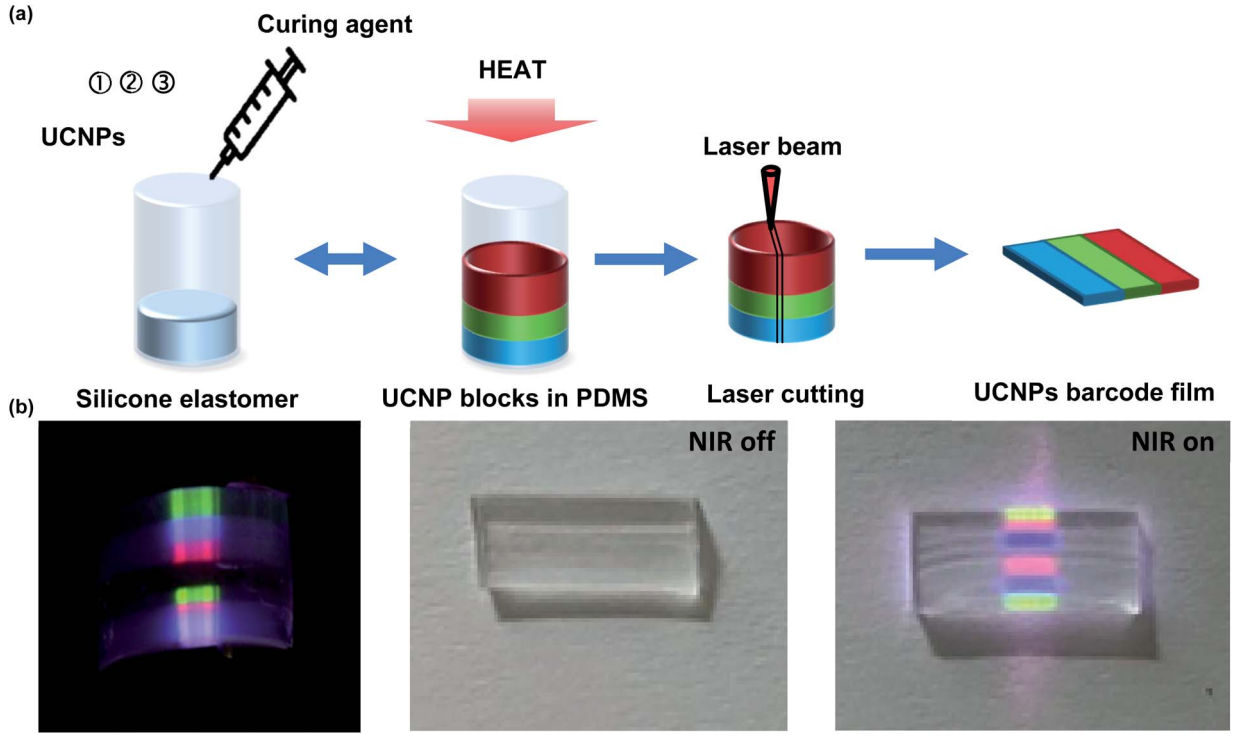

Fig. 5 (a) Schematic illustration for the fabrication process of transparent UCNPs barcode films. (b) Photographs showing (left) the fabricated UCNPs-PDMS composite layers in a cylindrical mold, the UCNPs barcode patch (middle) without and (right) with 980 nm NIR light irradiation (500 mW cm^{-2}).

analyzed RGB values, and code 0 to the blank (PDMS only). The embedded UCNPs emitted distinct RGB colors, indicating the feasibility for the application to barcode systems.

UCNPs barcode films were fabricated by a simple stacking method of UCNPs-PDMS composite layer with a specific sequence of multispectral patterns under 980 nm NIR (Fig. 5). Using this simple and fast fabrication method, it was possible to produce many of transparent barcode films with a specific sequence. As a model prototype, we fabricated a barcode film with the order of green-blue-red-blank-blue-red-green specific sequence of pattern by the simple stacking method. Fig. 5a shows the fabrication process of the barcode film by 4 steps. First, bUCNPs were dispersed in the silicone elastomer and crosslinked with a curing agent in a circular mold for 30 min. After that, gUCNPs and rUCNPs embedded PDMS were sequentially fabricated on the bUCNPs-embedded PDMS. The fabricated PDMS layers were taken out from the mold and cut into thin films using a laser cutter. We confirmed that UCNPs-PDMS composites were cured in the predetermined order in the cylindrical mold. The UCNPs-PDMS composites layer was in the order of green-blue-red-blank-blue-red-green under 980 nm NIR (Fig. 5b). In addition, we confirmed that the film had high transparency without NIR light, indicating the feasibility for the application to contact lens.

According to the above fabricating and encoding process, we designed a graphical/spectral-hybrid decodable platform. We prepared four 7-digit barcode films fabricated by the simple stacking method and encoded each film with unique codes as

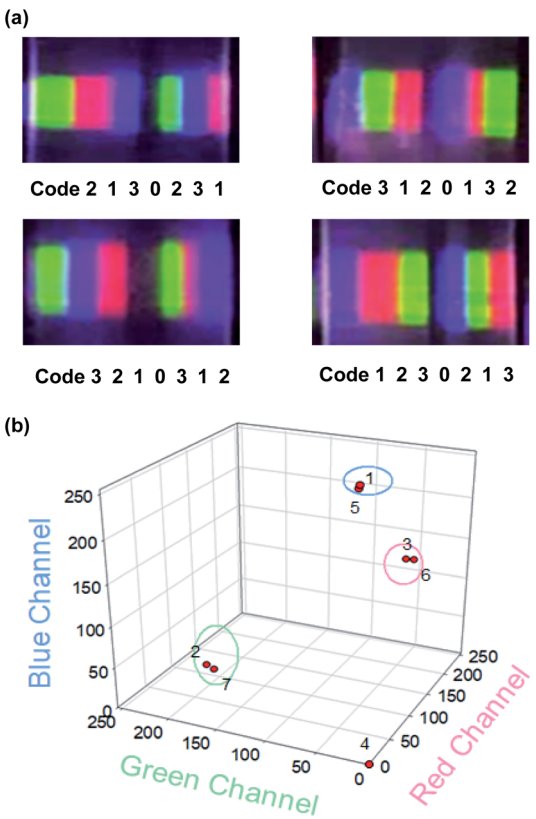

Fig. 6 (a) Photoimages of 7-digit barcode patches under 980 nm light (500 mW cm^{-2}) and the assigned codes. (b) The decoding plot for the assigned code of '3210312' in the 3D RGB channel map.

specific spectral barcode patterns for 0 to blank (PDMS only), code 1 (rUCNPs-PDMS), code 2 (gUCNPs-PDMS), and code 3 (bUCNPs-PDMS) under 980 nm NIR light (Fig. 6a). One of the fabricated transparent UCNPs barcode film, 'code 3210312' was decoded with a CCD camera. The emission spectra of UCNPs barcode film were converted to a unique code which was previously assigned by the RGB value analysis. Subsequently, the order of each code was recognized with the previously fabricated sequence in 3D RGB channel map as shown in Fig. 6b. Based on 4 digits of codes (code 0, 1, 2, 3), this decodable UCNPs barcode platform could increase the scale of encoding capacities exponentially [$>N^x$ where N: the number of selected colors, x: the number of code digits] depending on selected color numbers and sequence numbers. For example, we demonstrate 7 digits of codes with selected 3 of colors and blank [Fig. 6a]. In addition, our UCNPs barcode film could be readout under 980 nm NIR irradiation without interference to the visible light.

As a compact wearable individual recognition platform, we applied UCNPs barcode films in a contact lens. The UCNPs-BCL was fabricated to contain the UCNPs barcode film. The fabricated UCNPs barcode film was cut into small size and successfully embedded in the edge of the contact lens mold during the fabrication of contact lens. The prepared UCNPS-BCL showed sufficient transparency and upconversion emission of fabricated pattern under 980 nm NIR. As shown in Fig. 7a, the letters under the fabricated contact lens were clearly visible with transparency. In a dark condition, the 7-digit RGB light combination barcode was observed on the contact lens under 980 nm laser irradiation (Fig. 7b). This fabricated contact lens showed a green-blue-red-blank-blue-red-green color in the ordered sequence, and this barcode pattern was interpreted as 'code 3210312' by the CCD camera. Since each code can be assigned to a specific subject, a human recognition system would be developed by analyzing the code in a contact lens. In addition, because each individual has a distinctive iris shape just like fingerprints, the combination of our UCNPs barcode film platform and iris recognition system would be used as a robust wearable individual recognition platform. Furthermore, to assess the feasibility of our UCNPs barcode film for practical applications, we applied UCNPs barcode films to attachable patch and various substrates. They were successfully applied on the porcine skin and a paper currency as shown in Fig. 7c and d. The UCNPs barcode patches on various substrates were clearly readable with the CCD camera under NIR light irradiation. In addition, the sequences of barcode color patterns were recognizable enough to decode by using a CCD. All these results demonstrated the possibility of multispectral UCNPs transparent films for the applications to wearable individual recognition and non-face-to-face authorization.

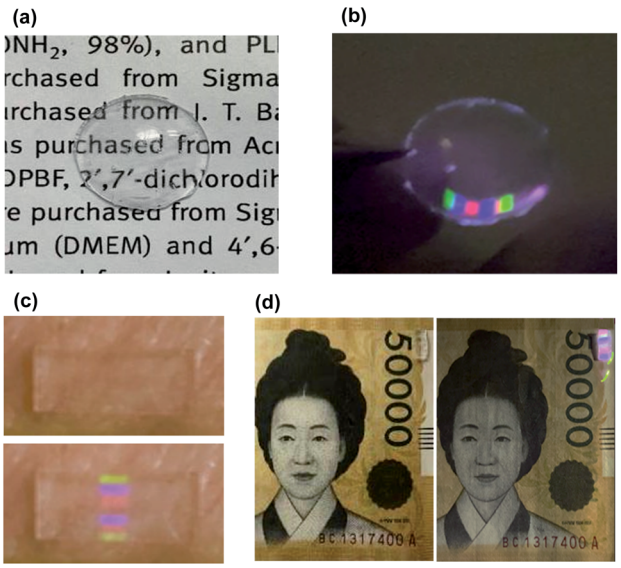

Fig. 7 Photoimages of UCNPs-barcode patterned contact lens on letters under (a) indoor-room light and (b) 980 nm NIR light (500 mW cm^{-2}) in the dark field. Photoimages of UCNPs barcode patch on (c) porcine skin and (d) paper currency under indoor-room light and 980 nm NIR light.

Conclusions

We successfully developed the transparent multispectral UCNPs films as a potential encoded platform for individual recognition, livestock classification, counterfeit currency and so forth. TEM, EELS, DLS, spectrofluorometry and XRD analyses made clear the successful synthesis of multispectral RGB UCNPs. The transparent UCNPs barcode film was fabricated by simple stacking methods with high productivity and reproducibility at a low cost. The fabricated transparent UCNPs barcode film was encoded with specific codes for each color as unique optical properties of RGB values. Upon 980 nm NIR illumination, the barcode pattern could be successfully decoded with a CCD camera through RGB value analysis in sequence according to the assigned codes. Finally, we could apply this transparent UCNPs barcode film to wearable devices including a contact lens and a skin patch for facile individual recognition. Taken together, we could confirm the feasibility of multispectral UCNPs transparent films for the individual recognition and non-face-to-face authorization.

Conflicts of interest

There are no conflicts to declare.

Acknowledgements

This research was supported by the Basic Science Research Program (2020R1A2C3014070), the Korea Medical Device Development Fund grant (2020M3E5D8105732), and Bio & Medical Technology Development Program (2021M3E5E7021473) of the National Research Foundation (NRF) funded by the Ministry of Science and ICT, Korea.

References

1 D. Bhattacharyya, R. Ranjan, F. Alisherov and M. Choi, *International Journal of u- and e-Service, Science and Technology*, 2009, **2**(3), 13–28.

2 S. K. Devireddy, G. Ramaswamy, D. Ravikiran and P. S. Rani, *J. Theor. Appl. Inf. Technol.*, 2009, **5**(5), 531–537.
3 K. Juneja and C. Rana, *Wireless Pers. Commun.*, 2021, **116**(1), 267–300.
4 D. Kage, K. Hoffmann, G. Nifontova, V. Krivenkov, A. Sukhanova, I. Nabiev and U. Resch-Genger, *Sci. Rep.*, 2020, **10**(1), 1–11.
5 I. L. Medintz, H. T. Uyeda, E. R. Goldman and H. Mattoussi, *Nat. Mater.*, 2005, **4**, 435–446.
6 C. D. Keating and M. J. Natan, *Adv. Mater.*, 2003, **15**, 451–454.
7 M. J. Dejneka, A. Streltsov, S. Pal, A. G. Frutos, C. L. Powell, K. Yost, P. K. Yuen, U. Müller and J. Lahiri, *Proc. Natl. Acad. Sci. U.S.A.*, 2003, **100**(2), 389–393.
8 F. Zhang, Q. Shi, Y. Zhang, Y. Shi, K. Ding, D. Zhao and G. D. Stucky, *Adv. Mater.*, 2011, **23**, 3775–3779.
9 X. Liu, Z. H. Chen, H. Zhang, Y. Fan and F. Zhang, *Angew. Chem., Int. Ed.*, 2021, **60**(13), 7041–7045.
10 H. Zhang, Y. Fan, P. Pei, C. Sun, L. Lu and F. Zhang, *Angew. Chem., Int. Ed.*, 2019, **58**(30), 10153–10157.
11 L. Zhou, Y. Fan, R. Wang, X. Li, L. Fan and F. Zhang, *Angew. Chem., Int. Ed.*, 2018, **57**(39), 12824–12829.
12 D. C. Pregibon, M. Toner and P. S. Doyle, *Science*, 2007, **315**(5817), 1393–1396.
13 S. Müssig, J. Reichstein, J. Prieschl, S. Wintzheimer and K. A. Mandel, *Small*, 2021, 2101588.
14 K. Cederquist, S. Dean and C. Keating, *Nanobiotechnol*, 2010, **2**, 578–600.
15 K. Braeckmans, S. C. De Smedt, M. Leblans, R. Pauwels and J. Demeester, *Nat. Rev. Drug Discov.*, 2002, **1**, 447–456.
16 R. Wilson, A. R. Cossins and D. G. Spiller, *Angew. Chem., Int. Ed.*, 2006, **45**, 6104–6117.
17 H. Lee, J. Kim, H. Kim and S. Kwon, *Nat. Mater.*, 2010, **9**, 745–749.
18 S. R. Nicewarner-Pena, R. G. Freeman, B. D. Reiss, L. He, D. J. Peña, I. D. Walton, R. Cromer, C. D. Keating and M. J. Natan, *Science*, 2001, **294**(5540), 137–141.
19 C. Lin, R. Jungmann, A. M. Leifer, C. Li, D. Levner, G. M. Church, W. M. Shih and P. Yin, *Nat. Chem.*, 2012, **4**(10), 832–839.
20 D. Appleyard, S. Chapin, R. Srinivas and P. Doyle, *Nat. Protoc.*, 2011, **6**, 1761–1774.
21 X. Zeng, S. K. Vanga, E. T. Poh, Y. Shi, C. H. Sow, A. A. Bettiol and X. Liu, *Adv. Opt. Mater.*, 2020, **8**, 2001168.
22 Y. Fan, S. Wang and F. Zhang, *Angew. Chem., Int. Ed.*, 2019, **58**, 13208.
23 Z. Yi, Z. Luo, X. Qin, Q. Chen and X. Liu, *Acc. Chem. Res.*, 2020, **53**, 2692–2704.
24 N. M. Idris, M. K. Gnanasammandhan, J. Zhang, P. C. Ho, R. Mahendran and Y. Zhang, *Nat. Med.*, 2012, **18**, 1580–1585.
25 C. Wang, H. Tao, L. Cheng and Z. Liu, *Biomaterials*, 2011, **32**, 6143–6154.
26 X. Zhu, W. Feng, J. Chang, Y. W. Tan, J. Li, M. Chen, Y. Sun and F. Li, *Nat. Commun.*, 2016, **7**, 10437.
27 S. Han, B. W. Hwang, E. Y. Jeon, D. Jung, G. H. Lee, D. H. Keum, K. S. Kim, S. H. Yun and S. K. Hahn, *ACS Nano*, 2017, **11**(10), 9979–9988.
28 G. Hong, J. C. Lee, J. T. Robinson, U. Raaz, L. Xie, N. F. Huang, J. P. Cooke and H. Dai, *Nat. Med.*, 2012, **18**, 1841–1848.
29 L. Cheng, K. Yang, Y. Li, X. Zeng, M. Shao, S. T. Lee and Z. Liu, *Biomaterials*, 2012, **33**, 2215–2222.
30 Y. Fan, P. Wang, Y. Lu, R. Wang, L. Zhou, X. Zheng, X. Li, J. a. Piper and F. Zhang, *Nat. Nanotechnol.*, 2018, **13**(10), 941–946.
31 G. H. Lee, H. Moon, H. Kim, G. H. Lee, W. Kwon, S. Yoo, D. Myung, S. H. Yun, Z. Bao and S. K. Hahn, *Nat. Rev. Mater.*, 2020, 1–17.
32 S. Han, W. Sung, T. Y. Kim, S. J. Yang, S. Kim, G. Lee, K. Cho and S. K. Hahn, *Nano Energy*, 2020, 105650.
33 C. Wang, X. Li and F. Zhang, *Analyst*, 2016, **141**(12), 3601–3620.
34 H. Liu, J. Xu, H. Wang, Y. Liu, Q. Ruan, Y. Wu, L. Xiaogang and J. K. Yang, *Adv. Mater.*, 2019, **31**(15), 1807900.
35 J. Kim, M. Kim, M.-S. Lee, K. Kim, S. Ji, Y.-T. Kim, J. Park, K. Na, K.-H. Bae, H. K. Kim, F. Bien, C. Y. Lee and J.-U. Park, *Nat. Commun.*, 2017, **8**, 14997.
36 J. Park, J.-H. Kim, S.-Y. Kim, W. H. Cheong, J. Jang, Y.-G. Park, K. Na, Y.-T. Kim, J. H. Heo, C. Y. Lee, J. H. Lee, F. Bien and J.-U. Park, *Sci. Adv.*, 2018, **4**, eaap9841.
37 J. Mun, J. won Mok, S. Jeong, S. Cho, C. K. Joo and S. K. Hahn, *RSC Adv.*, 2019, **9**(29), 16578–16585.
38 J. Shin, J. H. Kyhm, A. R. Hong, J. D. Song, K. Lee, H. Ko and H. S. Jang, *Chem. Mater.*, 2018, **30**(23), 8457–8464.
39 S. Li, Y. Meng, Y. Guo, T. Liu, S. Stavrakis, P. D. Howes and A. J. deMello, *J. Mater. Chem. C*, 2020, **9**, 925–933.
40 M. K. Gnanasammandhan, N. M. Idris, A. Bansal, K. Huang and Y. Zhang, *Nat. Protoc.*, 2016, **11**, 688–713.
41 Q. Chen, X. Xie, B. Huang, L. Liang, S. Han, Z. Yi, Y. Wang, Y. Li, D. Fan, L. Huang and X. Liu, *Angew. Chem., Int. Ed.*, 2017, **56**, 7605–7609.
42 S. Han, R. Deng, X. Xie and X. Liu, *Angew. Chem., Int. Ed.*, 2014, **53**(44), 11702–11715.